A Novel Modal Analysis of a Circular-to-Rectangular Waveguide T-Junction and Its Application to Design of Circular Waveguide Dual-Mode Filters

Ke-Li Wu, *Senior Member, IEEE*, Ming Yu, *Member, IEEE*, and Apu Sivadas

***Abstract*—This paper describes a novel modal analysis of a circular-to-rectangular waveguide T-junction and its application to the design of circular waveguide dual-mode filters with a sidewall coupling iris. The analysis is based on the newly developed finite plane-wave series-expansion technique and the concept of the extended boundary condition. The combination of the two concepts greatly facilitates the modal analysis of complex boundary value problems and eliminates the numerical integration. The proposed modal analysis has been verified both by experiments and commercial software for a wide range of parameters. Design examples of I/O structures for a set of channel filters demonstrate the great value of the new modal analysis scheme in practical applications.**

***Index Terms*—Antenna feeds, mode-matching method, waveguide components, waveguide filter.**

I. Introduction

In A communication satellite, the high-power amplifiers (HPAs) operate linearly only over a narrow band, necessitating the use of microwave multiplexers: 1) to channelize a wide-band signal prior to amplification (input multiplexer) and 2) to combine the amplified narrow-band signals prior to retransmission (output multiplexer). Multiplexers are critical components of a satellite payload and the tradeoffs between the performance and complexity of the narrow-band microwave channel filters are of major concern in order to maintain a minimum mass [1]. Particularly in an output multiplexer, the tradeoff is achieved by employing the circular-waveguide dual-mode (CWDM) cavity. A typical CWDM filter is the longitudinal in-line structure, in which the I/O coupling apertures are cut on the end walls. The modal analysis formulation for designing such I/O irises is well known and is given in [2]. To realize sophisticated electrical performance using symmetrical/asymmetrical canonical filter structures and to fully make use of any spare space, it becomes necessary to use the sidewall coupled irises from which filters are attached to the waveguide manifold, as shown in Fig. 1.

Since it involves a rectangular aperture on a curved cylindrical surface, designing the sidewall coupling iris is far more complicated than that of the end-coupled configurations. A formulation incorporating both cylindrical and rectangular coordinate systems needs to be considered. Due to the existence of the finite width of the sidewall coupling aperture that causes the couplings between the degenerate modes, the analysis formulation must explicitly include the two degenerate modes resonating in the cavity so that the coupling coefficient that is used in the filter design can be directly extracted. Furthermore, modal analysis is apt to provide the S-parameters among all the higher order modes of interest, in addition to the high accuracy (especially for narrow-bandwidth filter design) brought in by its nature of analytic solutions. This attribute is very important when the module is cascaded with other modal analysis modules in a systematic electromagnetic simulation.

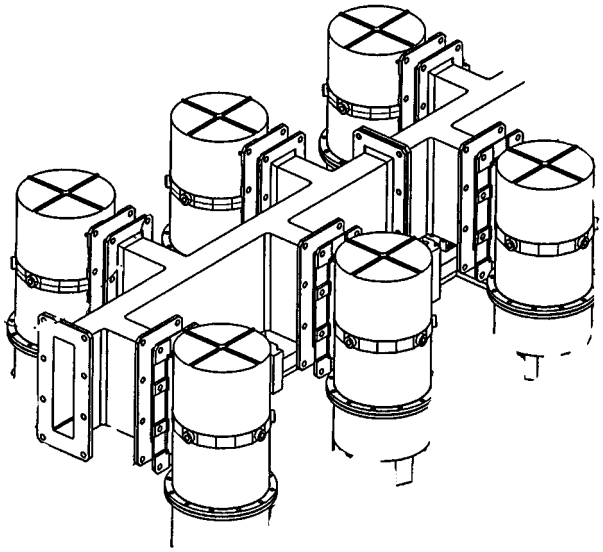

Fig. 1. Multiplexer assembly employing sidewall I/O coupled dual-mode filters.

The key module in designing the I/O coupling irises is a waveguide T-junction that has a rectangular waveguide arm branching out from a circular waveguide. The modal analysis of the T-junction is difficult due to the mixed boundary shape of curved and straight surfaces. Although many numerical methods such as the finite-element method (FEM) are available for the analysis of the key module, their lengthy computation time and the lack of sufficient higher order modes information that is crucial for the cascading with other key modules impel people to seek analytic modal analysis. An approximated modal analysis was proposed to solve the T-junction problem [3] and was further used for designing a waveguide orthomode

Manuscript received December 18, 2000.

K.-L. Wu is with the Department of Electronic Engineering, The Chinese University of Hong Kong, Shatin, Hong Kong.

M. Yu is with Corporate Research and Development, COM DEV International, Cambridge, ON, Canada, N1R 7H6.

A. Sivadas was with Corporate Research and Development, COM DEV International, Cambridge, ON, Canada, N1R 7H6. He is now with the GENNUM Corporation, Burlington, ON, Canada L7L 5P.

Publisher Item Identifier S 0018-9480(02)01153-5.

transducer [4]. In the approximated analysis, it is assumed that the radius of the circular waveguide is much greater than the height of the rectangular waveguide. Although this assumption restricts its applications to T-junctions with a thin longitudinal rectangular waveguide slot, it completely eliminates the numerical integration from the analysis. Other modal analysis schemes have also been proposed to tackle the T-junction problem by legitimate mathematical treatments. For example, an intermediate transition region between a rectangular waveguide and circular waveguide was introduced to facilitate the analysis in [5], and the generalized admittance matrix (GAM) was determined by wisely choosing the expansion and testing functions [6]. Nevertheless, numerical integration is inevitable in these modal analysis schemes and deteriorates the overall accuracy of a system simulation, which is particularly important when a thin iris is cascaded with the rectangular aperture of the T-junction.

In this paper, we present a new modal analysis called the extended boundary condition modal analysis (EBMA) for solving the T-junction problem. The analysis employs the finite plane-wave series-expansion technique [7] and matches the boundary conditions on the extended virtual planar boundary that interfaces with the rectangular waveguide. Therefore, no numerical integration is required in the analysis for dealing with the field matching along the curved boundary. Since it is virtually an analytic solution, it can be used for wide rectangular opening on the sidewall of the circular waveguide. This feature is crucial for designing a dual-mode filter with high power-handling capability. The outline of the theoretical analysis will be given in Section II. The model has been validated by comparing the modal analysis results with those of both experiments and computer simulations with commercial finite-element software. Excellent agreement has been achieved in all the cases.

II. Formulations

A. EBMA

The structure of the T-junction and the coordinate system are shown in Fig. 2. To use the resonant-mode technique [9], the T-junction is divided into the following four subregions:

- $WG1$ (bounded by S_3 and the right section of the circular waveguide);
- $WG3$ (bounded by S_1 and the left section of the circular waveguide);
- $WG2$ (bounded by S_2 and the rectangular waveguide section);
- cavity region Cav, a section of circular waveguide ended by S_1 and S_3.

The electric and magnetic fields in $WG1$ and $WG3$ can be expressed in terms of the eigenmode functions in cylindrical coordinates. The fields in $WG2$ are expressed in terms of the eigenmode functions in a local rectangular coordinates. The fields in the cavity region Cav are the superposition of three types of field solutions: solutions 1 and 2 correspond to the problems with S_2' and S_3, and S_2' and S_1 short circuited, respectively; and solution 3 corresponds to the case of parallel plates with S_1 and S_3 short circuited.

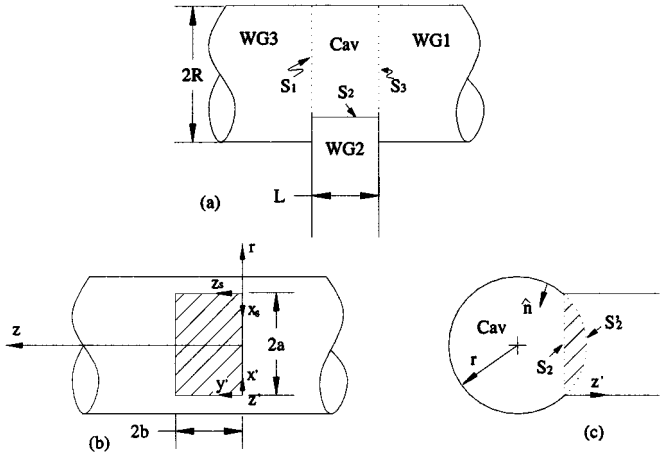

Fig. 2. Perspective views of the circular to rectangular T-junction.

It should be noted that there are two possible dividing boundary surfaces between the rectangular waveguide $WG2$ and the circular waveguide section. The first possible dividing boundary is naturally curved surface S_2'. The second possible dividing boundary is S_2, plus two crescent-shaped fragments—one is on S_1 and another is on S_3. Obviously, if the fields in the cavity region match with the fields in the rectangular waveguide on the planar surface S_2 and the two crescent-shaped fragments, the fields must match on the curved surface S_2'. To avoid unnecessary numerical integration and simplify the analysis, the field continuity condition over the two crescent-shaped areas is omitted in matching the fields between the cavity region and the $WG2$ region. It is postulated that this omission does not affect the analysis if the width of the aperture is not oversized since the matching of the fields in Cav and those in $WG1$ and $WG3$ over the areas is enforced. The numerical results have shown that the postulate is valid for most of the practical applications.

Therefore, instead of matching the field continuity on S_2', the proposed modal analysis matches the fields on the planar surface S_2. In order to match the fields on the circular apertures S_1 and S_3, as well as S_2, the field expressions in the cavity region take two different forms. One is in cylindrical coordinate system for matching the fields on S_1 and S_3. The other is in the rectangular coordinate system for facilitating the matching of the fields of the cavity region to that of the rectangular waveguide.

B. Modal Functions in Subregions

The modal functions of the electric field in circular waveguide 1 can be found in standard textbooks and are repeated here for completeness as follows:

$$\vec{e}_q^{1h} = N_{nm}^{1h}\left[\hat{r}\frac{n}{r}J_n\left(k_{nm}^h r\right)\begin{pmatrix}\sin(n\phi)\\ -\cos(n\phi)\end{pmatrix} + \hat{\phi}k_{nm}^h J_n'\left(k_{nm}^h r\right)\begin{pmatrix}\cos(n\phi)\\ \sin(n\phi)\end{pmatrix}\right] \quad (1a)$$

for TE modes, and

$$\vec{e}_q^{1e} = N_{nm}^{1e}\left[\hat{r}k_{nm}^e J_n'(k_{nm}^e r)\begin{pmatrix}-\cos(n\phi)\\ \sin(n\phi)\end{pmatrix} + \hat{\phi}\frac{n}{r}J_n\left(k_{nm}^e r\right)\begin{pmatrix}\sin(n\phi)\\ \cos(n\phi)\end{pmatrix}\right] \quad (1b)$$

for TM modes, where the superscripts h and e refer to TE and TM modes, respectively, and N_{nm} is the normalization factor. The combined index q corresponds to the integer mode index pair (n, m).

The modal functions of the electric field in rectangular wave 2 can be expressed as

$$\vec{e}_k^{2h} = N_{st}^{2h}\left[\left(\frac{t\pi}{2b}\right)\cos\left(\frac{s\pi}{2a}x'\right)\sin\left(\frac{t\pi}{2b}y'\right)\hat{x}' - \left(\frac{s\pi}{2a}\right)\sin\left(\frac{s\pi}{2a}x'\right)\cos\left(\frac{t\pi}{2b}y'\right)\hat{y}'\right] \quad (2a)$$

for TE modes, and

$$\vec{e}_k^{2e} = N_{st}^{2e}\left[\left(\frac{s\pi}{2a}\right)\cos\left(\frac{s\pi}{2a}x'\right)\sin\left(\frac{t\pi}{2b}y'\right)\hat{x}' + \left(\frac{t\pi}{2b}\right)\sin\left(\frac{s\pi}{2a}x'\right)\cos\left(\frac{t\pi}{2b}y'\right)\hat{y}'\right] \quad (2b)$$

for TM modes, where k is the combined mode index corresponding to the integer mode index pair (s, t).

It is straightforward to show using transmission-line theory and Maxwell's equations that when S_1 is short circuited, the TE modal functions of electric and magnetic fields are given by

$$\vec{\Phi}_q^{1h} = \vec{e}_q^{1h} sh\big[\gamma(z-L)\big] \quad (3a)$$

$$\vec{\Psi}_q^{1h} = -\frac{\gamma}{j\omega\mu_0}\left(\hat{z}\times\vec{e}_q^{1h}\right)ch\big[\gamma(z-L)\big] + \hat{z}\frac{N_{nm}^{1h}}{j\omega\mu_0}\left(k_{nm}^h\right)^2 \cdot J_n\left(k_{nm}^h r\right)\begin{pmatrix}\cos(n\phi)\\ \sin(n\phi)\end{pmatrix} sh\big[\gamma(z-L)\big] \quad (3b)$$

respectively. Similarly, one can find the TM modal functions of electric and magnetic fields, respectively, as

$$\vec{\Phi}_q^{1e} = \vec{e}_q^{1e} sh\big[\gamma(z-L)\big] - \hat{z}\frac{N_{nm}^{1e}}{\gamma}\left(k_{nm}^e\right)^2 \cdot J_n\left(k_{nm}^e r\right)\begin{pmatrix}\cos(n\phi)\\ -\sin(n\phi)\end{pmatrix} ch\big[\gamma(z-L)\big] \quad (4a)$$

$$\vec{\Psi}_q^{1e} = -\frac{j\omega\varepsilon_0}{\gamma}\left(\hat{z}\times\vec{e}_q^{1e}\right)ch\big[\gamma(z-L)\big]. \quad (4b)$$

The modal functions given in (3) and (4) can also be expressed in the rectangular coordinate system $(\hat{x}_s, \hat{y}_s, \hat{z}_s)$ through the finite plane-wave series expansion [2]. Since the tangential components of the fields on S_2 will be used, only the field components tangential to S_2 are given here.

For TE modes,

$$\Phi_{q,x_s}^{1h} = N_{nm}^{1h}A_{mn}\sum_{l=0}^{N-1} S_{ls}\begin{pmatrix}C_{ln}\\ S_{\ln}\end{pmatrix} \cdot E_{mls}e^{-jk_{nm}^h C_{ls}x_s} sh\big[\gamma(z-L)\big] \quad (5a)$$

$$\Psi_{q,x_s}^{1h} = N_{nm}^{1h}\left(\frac{-\gamma}{j\eta_0 k_0}\right)A_{mn}\sum_{l=0}^{N-1} C_{ls}\begin{pmatrix}C_{\ln}\\ S_{\ln}\end{pmatrix} \cdot E_{mls}e^{-jk_{nm}^h C_{ls}x_s} ch\big[\gamma(z-L)\big] \quad (5b)$$

$$\Psi_{q,z_s}^{1h} = N_{nm}^{1h}\left(\frac{k_{nm}^h}{j\eta_0 k_0}\right)\frac{1}{j}A_{mn}\sum_{l=0}^{N-1}\begin{pmatrix}C_{\ln}\\ S_{\ln}\end{pmatrix} \cdot E_{mls}e^{-jk_{nm}^h C_{ls}x_s} sh\big[\gamma(z-L)\big] \quad (5c)$$

and for TM modes,

$$\Phi_{q,x_s}^{1e} = N_{nm}^{1e}A_{mn}\sum_{l=0}^{N-1} C_{ls}\begin{pmatrix}C_{\ln}\\ -S_{\ln}\end{pmatrix} \cdot E_{mls}e^{-jk_{nm}^e C_{ls}x_s} sh\big[\gamma(z-L)\big] \quad (6a)$$

$$\Phi_{q,z_s}^{1e} = N_{nm}^{1e}\left(\frac{-k_{nm}^e}{j\gamma}\right)A_{mn}\sum_{l=0}^{N-1}\begin{pmatrix}C_{\ln}\\ -S_{\ln}\end{pmatrix} \cdot E_{mls}e^{-jk_{nm}^e C_{ls}x_s} ch\big[\gamma(z-L)\big] \quad (6b)$$

$$\Psi_{q,x_s}^{1e} = N_{nm}^{1e}\left(\frac{-jk_0}{\eta_0\gamma}\right)A_{mn}\sum_{l=0}^{N-1} S_{ls}\begin{pmatrix}-C_{\ln}\\ S_{\ln}\end{pmatrix} \cdot E_{mls}e^{-jk_{nm}^e C_{ls}x_s} ch\big[\gamma(z-L)\big]. \quad (6c)$$

The details of constants A_{nm}, $C_{\ln}$, $S_{\ln}$ and E_{mls} are given in [2] and [7].

By the same token, the modal functions for the case in which S_3 is short circuited can be obtained. The modal functions are very similar to those in (3)–(6), except that the parameter L is set to zero and that superscript 1 is replaced by 3.

C. Field Expansions and the Field-Matching Procedure

It is well known that the total fields in any waveguide section can be expressed as a linear superposition of TE and TM modes with respect to a homogeneous direction. Therefore, the total field at waveguide ports 1–3 are expressed as

$$\vec{E}_t^{(i)} = \sum_l\left(a_{h,l}^{(i)} + b_{h,l}^{(i)}\right)\sqrt{Z_{h,l}^{(i)}}\,\vec{e}_l^{ih} + \sum_l\left(a_{e,l}^{(i)} + b_{e,l}^{(i)}\right)\sqrt{Z_{e,l}^{(i)}}\,\vec{e}_l^{ie} \quad (7a)$$

$$\vec{H}_t^{(i)} = \sum_l\left(\begin{Bmatrix}1\\ -1\\ -1\end{Bmatrix}a_{h,l}^{(i)} + \begin{Bmatrix}-1\\ 1\\ 1\end{Bmatrix}b_{h,l}^{(i)}\right)\cdot\frac{1}{\sqrt{Z_{h,l}^{(i)}}}\left(\begin{Bmatrix}\hat{z}\\ \hat{z}'\\ \hat{z}\end{Bmatrix}\times\vec{e}_l^{ih}\right) + \sum_l\left(\begin{Bmatrix}1\\ -1\\ -1\end{Bmatrix}a_{e,l}^{(i)} + \begin{Bmatrix}-1\\ 1\\ 1\end{Bmatrix}b_{e,l}^{(i)}\right)\cdot\frac{1}{\sqrt{Z_{e,l}^{(i)}}}\left(\begin{Bmatrix}\hat{z}\\ \hat{z}'\\ \hat{z}\end{Bmatrix}\times\vec{e}_l^{ie}\right) \quad (7b)$$

where $i = 1, 2, 3$, a and b are the mode coefficients of incident and reflected waves, respectively, and Z is the wave impedance of the corresponding mode.

The total fields in the cavity region are expressed as a linear combination of three types of modes (each in TE and TM) with respect to the z-direction as follows:

$$\vec{E}^{(4)} = \sum_l C^h_{1,l}\vec{\Phi}^{1h}_l + \sum_l C^e_{1,l}\vec{\Phi}^{1e}_l + \sum_l C^h_{2,l}\vec{\Phi}^{2h}_l + \sum_l C^e_{2,l}\vec{\Phi}^{2e}_l + \sum_l C^h_{3,l}\vec{\Phi}^{3h}_l + \sum_l C^e_{3,l}\vec{\Phi}^{3e}_l \quad (8a)$$

$$\vec{H}^{(4)} = \sum_l C^h_{1,l}\vec{\Psi}^{1h}_l + \sum_l C^e_{1,l}\vec{\Psi}^{1e}_l + \sum_l C^h_{2,l}\vec{\Psi}^{2h}_l + \sum_l C^e_{2,l}\vec{\Psi}^{2e}_l + \sum_l C^h_{3,l}\vec{\Psi}^{3h}_l + \sum_l C^e_{3,l}\vec{\Psi}^{3e}_l \quad (8b)$$

where $\vec{\Phi}^{1(h,e)}_l$, $\vec{\Phi}^{3(h,e)}_l$, $\vec{\Psi}^{1(h,e)}_l$ and $\vec{\Psi}^{3(h,e)}_l$ are given by (3)–(6) and $\vec{\Phi}^{2(h,e)}_l$ and $\vec{\Psi}^{2(h,e)}_l$ are the mode functions of a parallel-plate waveguide with plate spacing L. The plane-wave expansions of the mode functions for the parallel-plate waveguide are given in [7] and will be used to match the field at S_2. The expression of the mode functions in cylindrical coordinate system will be used to force the tangential electric field on the wall of the circular cavity to zero.

The electric-field continuity at S_1 is enforced by taking inner product of the electric-field matching equations with $\vec{e}^{1h}_k$ and $\vec{e}^{1e}_k$ across the circular waveguide cross section. The same procedure is applied to enforce the electric-field continuity at S_3.

The electric-field continuity at S_2 is enforced by matching the electric fields on both sides of the planar surface, i.e.,

$$\sum_l \left(a^{(2)}_{h,l} + b^{(2)}_{h,l}\right)\sqrt{Z^{(2)}_{h,l}}\vec{e}^{2h}_l + \sum_l \left(a^{(2)}_{e,l} + b^{(2)}_{e,l}\right)\sqrt{Z^{(2)}_{e,l}}\vec{e}^{2e}_l = \left\{\sum_l C^h_{1,l}\vec{\Phi}^{1h}_l + \sum_l C^e_{1,l}\vec{\Phi}^{1e}_l + \sum_l C^h_{2,l}\vec{\Phi}^{2h}_l + \sum_l C^e_{2,l}\vec{\Phi}^{2e}_l + \sum_l C^h_{3,l}\vec{\Phi}^{3h}_l + \sum_l C^e_{3,l}\vec{\Phi}^{3e}_l\right\}_{S2} \quad (9)$$

by taking the inner product of (9) with $\vec{\Psi}^{2h}_l$ and $\vec{\Psi}^{2e}_l$, respectively. Since S_2 is a planar surface, the mode functions of Φs in a rectangular coordinate format need to be used in the field-matching procedure. As discussed earlier, the mode functions $\vec{\Phi}^{1(h,e)}$ and $\vec{\Phi}^{3(h,e)}$ given by (5) are obtained by finite plane-wave series expansion. The mode functions $\vec{\Psi}^{2h}$ and $\vec{\Psi}^{2e}$ of a parallel-plate waveguide in rectangular coordinates are developed in [7].

The matching of electric field at ports 1–3, as well as the enforcement of the tangential electric field to zero on the conducting sidewall of the cavity region, lead to the following matrix equation:

$$\underbrace{\begin{bmatrix} [I] & 0 & 0 & 0 & 0 & 0 \\ 0 & [I] & 0 & 0 & 0 & 0 \\ 0 & 0 & [E_2^{hh}] & [E_2^{eh}] & 0 & 0 \\ 0 & 0 & [E_2^{he}] & [E_2^{ee}] & 0 & 0 \\ 0 & 0 & 0 & 0 & [I] & 0 \\ 0 & 0 & 0 & 0 & 0 & [I] \end{bmatrix}}_{[E]} \begin{Bmatrix} a_h^{(1)} + b_h^{(1)} \\ a_e^{(1)} + b_e^{(1)} \\ a_h^{(2)} + b_h^{(2)} \\ a_e^{(2)} + b_e^{(2)} \\ a_h^{(3)} + b_h^{(3)} \\ a_e^{(3)} + b_e^{(3)} \end{Bmatrix} = \underbrace{\begin{bmatrix} [H_{11}^{hh}] & 0 & 0 & 0 & 0 & 0 \\ 0 & [H_{11}^{ee}] & 0 & 0 & 0 & 0 \\ [H_{21}^{hh}] & [H_{21}^{he}] & [H_{22}^{hh}] & [H_{22}^{eh}] & [H_{23}^{hh}] & [H_{23}^{eh}] \\ 0 & 0 & 0 & 0 & [H_{33}^{hh}] & 0 \\ 0 & 0 & 0 & 0 & 0 & [H_{33}^{ee}] \end{bmatrix}}_{[H]} \cdot \begin{Bmatrix} C_1^h \\ C_1^e \\ C_2^h \\ C_2^e \\ C_3^h \\ C_3^e \end{Bmatrix} \quad (10)$$

where the definition of the sub-matrices are given in the Appendix.

The magnetic-field continuity is sought only on waveguide apertures. The magnetic-field matching equations at S_1 and S_3 are projected to a set of linear equations by using $\vec{e}^{1h}_k$ and $\vec{e}^{1e}_k$ as testing functions. The magnetic-field continuity at planar surface S_2 is enforced by taking inner product of the magnetic-field continuity equation with $\vec{\Psi}^{2h}$ and $\vec{\Psi}^{2e}$. Due to the mode orthogonality in the circular waveguide, the above-mentioned procedures lead to the following matrix equation:

$$\begin{Bmatrix} a_h^{(1)} - b_h^{(1)} \\ a_e^{(1)} - b_e^{(1)} \\ a_h^{(2)} - b_h^{(2)} \\ a_e^{(2)} - b_e^{(2)} \\ a_h^{(3)} - b_h^{(3)} \\ a_e^{(3)} - b_e^{(3)} \end{Bmatrix} = \underbrace{\begin{bmatrix} [M_{11}^{hh}] & [\ 0\ ] & [M_{12}^{hh}] & [M_{12}^{he}] & [M_{13}^{hh}] & [\ 0\ ] \\ [\ 0\ ] & [M_{11}^{ee}] & [M_{12}^{eh}] & [M_{12}^{ee}] & [\ 0\ ] & [M_{13}^{ee}] \\ [M_{21}^{hh}] & [M_{21}^{he}] & [M_{22}^{hh}] & [M_{22}^{he}] & [M_{23}^{hh}] & [M_{23}^{he}] \\ [M_{21}^{eh}] & [M_{21}^{ee}] & [M_{22}^{eh}] & [M_{22}^{ee}] & [M_{23}^{eh}] & [M_{23}^{ee}] \\ [M_{31}^{hh}] & [\ 0\ ] & [M_{32}^{hh}] & [M_{32}^{he}] & [M_{33}^{hh}] & [\ 0\ ] \\ [\ 0\ ] & [M_{31}^{ee}] & [M_{32}^{eh}] & [M_{32}^{ee}] & [\ 0\ ] & [M_{33}^{ee}] \end{bmatrix}}_{[M]} \cdot \begin{Bmatrix} C_1^h \\ C_1^e \\ C_2^h \\ C_2^e \\ C_3^h \\ C_3^e \end{Bmatrix}. \quad (11)$$

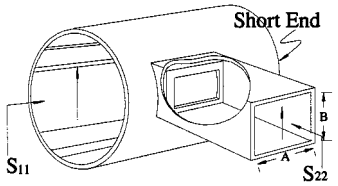

Fig. 3. Sidewall coupled circular waveguide cavity.

By eliminating the vector $\{C_1^h, C_1^e, C_2^h, C_2^e, C_3^h, C_3^e\}^T$ from (10) and (11), one obtains

$$\begin{Bmatrix} a_h^{(1)} - b_h^{(1)} \\ a_e^{(1)} - b_e^{(1)} \\ a_h^{(2)} - b_h^{(2)} \\ a_e^{(2)} - b_e^{(2)} \\ a_h^{(3)} - b_h^{(3)} \\ a_e^{(3)} - b_e^{(3)} \end{Bmatrix} = [M][H]^{-1}[E] \begin{Bmatrix} a_h^{(1)} + b_h^{(1)} \\ a_e^{(1)} + b_e^{(1)} \\ a_h^{(2)} + b_h^{(2)} \\ a_e^{(2)} + b_e^{(2)} \\ a_h^{(3)} + b_h^{(3)} \\ a_e^{(3)} + b_e^{(3)} \end{Bmatrix}$$

$$= [C] \begin{Bmatrix} a_h^{(1)} + b_h^{(1)} \\ a_e^{(1)} + b_e^{(1)} \\ a_h^{(2)} + b_h^{(2)} \\ a_e^{(2)} + b_e^{(2)} \\ a_h^{(3)} + b_h^{(3)} \\ a_e^{(3)} + b_e^{(3)} \end{Bmatrix} \tag{12}$$

or

$$\{\mathbf{b}\} = [I + C]^{-1}[I - C]\{\mathbf{a}\} = [S]\{\mathbf{a}\} \tag{13}$$

where $[I]$ is the identity matrix, $\{\mathbf{a}\}$ and $\{\mathbf{b}\}$ are the column vectors of incident and reflected waves at waveguide ports, and $[S]$ is the generalized scattering matrix (GSM) of the rectangular-to-circular waveguide T-junction. It is worth mentioning that the extended boundary condition and the plane-wave series expansion on the planar surface of port 2 lead to all the matrix elements in the above equation being analytically evaluated.

III. Designing of the Sidewall I/O Coupling

With reference to Fig. 3, to simulate the I/O structure and to obtain the GSM using the modal analysis, two basic key modules need to be cascaded. One module is the circular-to-rectangular waveguide T-junction with one end of the circular waveguide short circuited. The other is the rectangular-waveguide double-plane junction, which has been extensively studied by many researchers. Once the GSM is obtained, the following three critical filter design parameters can be extracted.

1) The phase compensation
$$\psi_c = \frac{\angle S_{11}}{2}$$
which determines the cavity length by taking into account of the loading of the sidewall coupling iris on the cavity.
2) The I/O coupling coefficient
$$R = \frac{2}{\pi}\frac{1 - |S_{11}|}{1 + |S_{11}|}\left(\frac{f_0}{\Delta f}\right)\left(\frac{\lambda_g}{\lambda_0}\right)^2$$
which is a parameter in the filter prototype, determined in the filter synthesis stage.
3) The phase compensation
$$\psi_m = \frac{\angle S_{22}}{2}$$
which is used for determining the spacing between the filter and waveguide manifold connecting to port 2 of the filter.

where S_{11} is the reflection coefficient of the vertically polarized TE_{11} mode at the circular waveguide port and the S_{22} refers to the reflection coefficient of the TE_{10} mode at the rectangular waveguide. The design procedure is to iterate the iris size until the I/O coupling coefficient matches the desired value. Strictly speaking, the calculation of I/O coupling coefficient involves the coupling coefficient of the two orthogonal modes in the cavity and the matching condition of the horizontal polarized TE_{11} mode of the circular waveguide cavity. For the case of a single pair of degenerate mode cavity or narrow slot coupled cavity, in which there is no energy transfer between modes, the above formulation for R is competent for most of the narrow bandwidth filter design. If there are more than one modes exist in the cavity or a wide slot coupled cavity such that the couplings between modes occur, like the calculation of the coupling coefficient of the two orthogonal modes in a cavity [8], more sophisticated procedure needs to be used to evaluate the I/O coupling coefficient using an electromagnetic simulation model.

This method of calculating the filter design parameters is valid only when the cavity diameter is in the range such that only the dominant TE_{11} mode is propagating inside the cavity. If the cavity is oversized for the purpose of a better quality factor, several higher order modes may be propagating inside the cavity. In that case, the coupling formulation would get far more sophisticated and would actually involve the use of the complete GSM of the coupling junction. This would be the subject of a future publication.

IV. Numerical Results

To verify the proposed EBMA, a circular waveguide cavity with a *narrow* longitudinal slot coupled to a rectangular waveguide is studied first. As illustrated in Fig. 4(a), the cavity consists of a circular-to-rectangular waveguide T-junction and two circular-to-rectangular waveguide end junctions that are used to facilitate the measurement. The calculated results using the proposed modal analysis are compared with the measurement results in Fig. 4(b). It can be seen that there is excellent agreement between the measurement and calculation.

In order to demonstrate the validity of the T-junction model for applications with a wide coupling slot, a circular waveguide cavity with a *wide* slot is also analyzed using the proposed model. The results are verified by those obtained from Ansoft's commercial HFSS software that is based on the FEM. Excellent agreement can be observed in Fig. 5. Since the electric performance at port 2 is critical for designing the input coupling of a dual-mode filter, the comparison of the magnified amplitudes of S_{22} and the phases of S_{22} are shown in Fig. 5(c) and (d), respectively. It is worthwhile to note that the largest discrepancy between the modal analysis result and that from

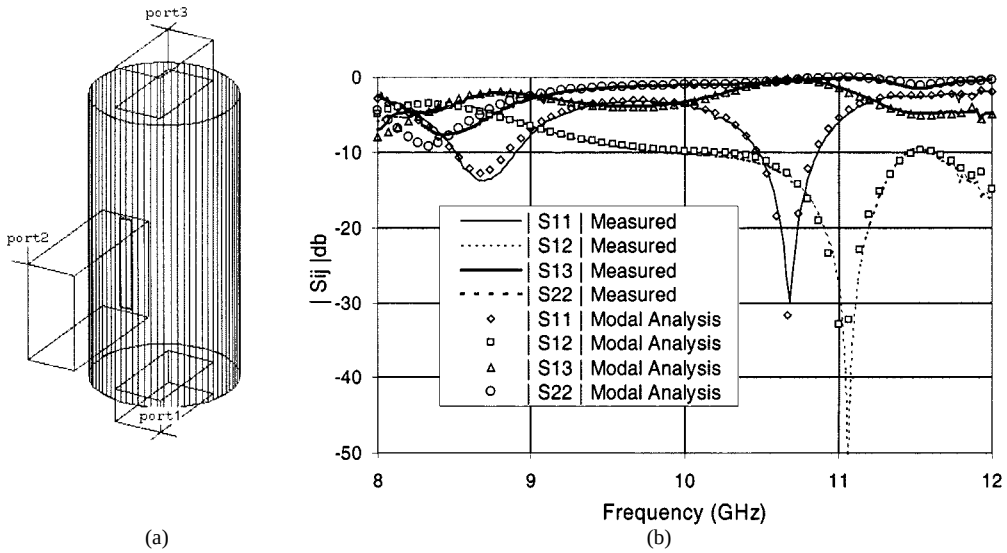

Fig. 4. Sidewall coupled circular cavity with a thin longitudinal rectangular slot. (a) Cavity structure. (b) Comparison of the measured and calculated amplitudes of S-parameters. The structure has the following details: radius of cavity $R = 0.535$, coupling iris thickness $t = 0.014$, coupling slot width $2a = 0.1$, coupling slot length $2b = 0.7$, cavity length $= 2.2$, the slot is located at the center of the cavity, and the WR 75 waveguide is used at each port. All the dimensions are in inches.

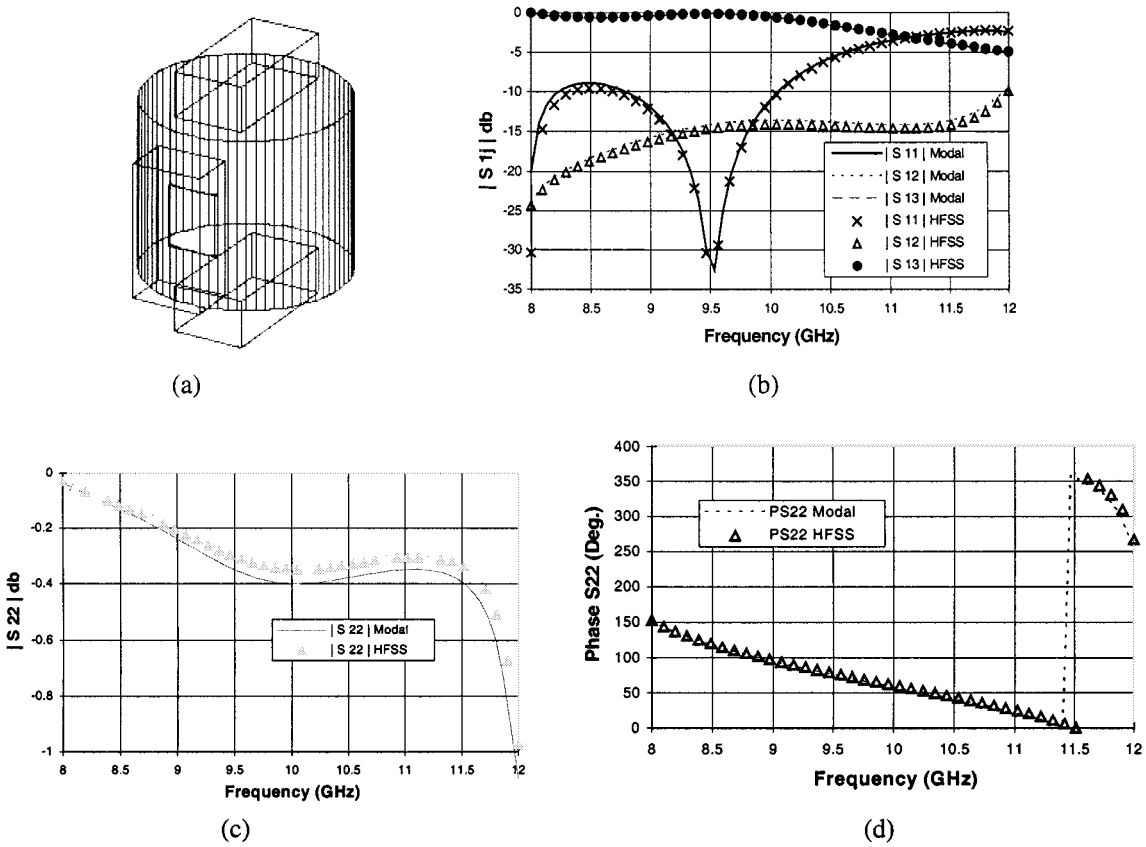

Fig. 5. Sidewall coupled circular cavity with a wide rectangular coupling slot. The waveguide port on the sidewall is defined as port 2 and the end ports are defined as ports 1 and 3. (a) Cavity structure. (b) Comparison of the S-parameters looking at port 1. (c) Comparison of the magnified amplitude of the reflection coefficient at port 2. (d) Comparison of phase of the reflection at port 2. The structure has the following details: radius of cavity $R = 0.525$, coupling iris thickness $t = 0.02$, coupling slot width $2a = 0.26$, coupling slot length $2b = 0.34$, cavity length $= 0.86$, the slot is located at the center of the cavity, and the WR 75 waveguide is used at each port. All the dimensions are in inches.

HFSS (for the magnitude of S_{22}) is less than 0.05 dB. Rectangular waveguides are used to cap the circular waveguide ends in order to enforce HFSS to consider the vertically polarized TE_{11} mode in the circular waveguide port.

The modal analysis results were used for designing a number of narrow-bandwidth channel filters with sidewall coupling. Table I summarizes the relevant parameters: the measured and the calculated I/O coupling coefficient R. Excellent

TABLE I
COMPARISONS OF THE CALCULATED AND MEASURED I/O COUPLING COEFFICIENT (R) OF NARROW-BANDWIDTH CHANNEL FILTERS WITH SIDEWALL COUPLING IRIS (ALL DIMENSIONS IN INCHES)

F_0 GHz	Cavity Length	Cavity Radius	Iris Length	Measured Coupling R	Calculated Coupling R
3.72	3.454	1.01	0.78	0.8043	0.7746
3.84	3.0579	1.01	0.705	0.5301	0.5475
4.04	3.0	0.95	0.643	0.6069	0.6058
4.08	2.907	0.95	0.599	0.3671	0.3682

agreement can be observed at large between measurement and computation, considering the fact that measurement error and mechanical dimension tolerance are also contributed in the deviation.

V. CONCLUSIONS

A new modal analysis for the circular to rectangular waveguide T-junction has been developed for designing CWDM filters with a sidewall coupling iris. The analysis is based on the finite plane-wave series-expansion technique and the concept of the extended boundary condition, which means that, if the fields are continuous over an artificial boundary surface in a continuous region, they must be continuous on the other surfaces in a continuous domain. This concept greatly facilitates the modal analysis of complex boundary value problems using modal analysis without involving any numerical integration. The proposed modal analysis has been verified both by experiments and finite-element simulation of commercial software in a wide range of parameters. A design example of practical channel filters using the proposed modal analysis has also been presented in this paper, demonstrating the great value of this modal analysis in practical applications.

Since the GSM of the T-junction is obtained in the proposed modal analysis, the model can be used in electromagnetic simulation and optimization of a waveguide circuit system involving the circular to rectangular T-junctions.

APPENDIX

$$E_2^{h(^h_e)}(k,l) = \left\langle \sqrt{Z_{h,l}^{(2)}}\vec{e}_l^{2h},\ \vec{\Psi}_k^{2(^h_e)} \right\rangle\Big|_{S2} = \sqrt{Z_{h,l}^{(2)}} \iint_{S2} \vec{e}_l^{2h} \times \vec{\Psi}_k^{2(^h_e)} \cdot \hat{n} ds$$

$$E_2^{e(^h_e)}(k,l) = \left\langle \sqrt{Z_{e,l}^{(2)}}\vec{e}_l^{2e},\ \vec{\Psi}_k^{2(^h_e)} \right\rangle\Big|_{S2} = \sqrt{Z_{e,l}^{(2)}} \iint_{S2} \vec{e}_l^{2e} \times \vec{\Psi}_k^{2(^h_e)} \cdot \hat{n} ds$$

$$H_{11}^{hh}(k,l) = \left\langle \vec{\Phi}_l^{1h},\ \hat{z} \times \vec{e}_k^{1h} \right\rangle\Big|_{S1} = \iint_{S1} \vec{\Phi}_l^{1h} \times \left(\hat{z} \times \vec{e}_k^{1h}\right) \cdot \hat{n} ds$$

$$H_{11}^{ee}(k,l) = \left\langle \vec{\Phi}_l^{1e},\ \hat{z} \times \vec{e}_k^{1e} \right\rangle\Big|_{S1} = \iint_{S1} \vec{\Phi}_l^{1e} \times \left(\hat{z} \times \vec{e}_k^{1e}\right) \cdot \hat{n} ds$$

$$H_{33}^{hh}(k,l) = \left\langle \vec{\Phi}_l^{3h},\ \hat{z} \times \vec{e}_k^{1h} \right\rangle\Big|_{S1} = \iint_{S3} \vec{\Phi}_l^{3h} \times \left(\hat{z} \times \vec{e}_k^{1h}\right) \cdot \hat{n} ds$$

$$H_{33}^{ee}(k,l) = \left\langle \vec{\Phi}_l^{3e},\ \hat{z} \times \vec{e}_k^{1e} \right\rangle\Big|_{S1} = \iint_{S3} \vec{\Phi}_l^{3e} \times (\hat{z} \times \vec{e}_k^{1e}) \cdot \hat{n} ds$$

$$H_{21}^{(^h_e)(^h_e)}(k,l) = \left\langle \vec{\Phi}_l^{1(^h_e)},\ \vec{\Psi}_k^{2(^h_e)} \right\rangle\Big|_{S2} = \iint_{S2} \vec{\Phi}_l^{1(^h_e)} \times \vec{\Psi}_k^{2(^h_e)} \cdot \hat{n} ds$$

$$H_{22}^{(^h_e)(^h_e)}(k,l) = \left\langle \vec{\Phi}_l^{2(^h_e)},\ \vec{\Psi}_k^{2(^h_e)} \right\rangle\Big|_{S2} = \iint_{S2} \vec{\Phi}_l^{2(^h_e)} \times \vec{\Psi}_k^{2(^h_e)} \cdot \hat{n} ds$$

$$H_{23}^{(^h_e)(^h_e)}(k,l) = \left\langle \vec{\Phi}_l^{3(^h_e)},\ \vec{\Psi}_k^{2(^h_e)} \right\rangle\Big|_{S2} = \iint_{S2} \vec{\Phi}_l^{3(^h_e)} \times \vec{\Psi}_k^{2(^h_e)} \cdot \hat{n} ds$$

$$M_{11}^{(^{hh}_{ee})}(l,k) = \sqrt{Z_{(^h_e)}^{(1)}} \left\langle \vec{e}_l^{1(^h_e)},\ \vec{\Psi}_k^{1(^h_e)} \right\rangle\Big|_{S1} = \sqrt{Z_{(^h_e)}^{(1)}} \iint_{S1} \vec{e}_l^{1(^h_e)} \times \vec{\Psi}_k^{1(^h_e)} \cdot \hat{n} ds$$

$$M_{12}^{h(^h_e)}(l,k) = \sqrt{Z_h^{(1)}} \left\langle \vec{e}_l^{1h},\ \vec{\Psi}_k^{2(^h_e)} \right\rangle\Big|_{S1} = \sqrt{Z_h^{(1)}} \iint_{S1} \vec{e}_l^{1h} \times \vec{\Psi}_k^{2(^h_e)} \cdot \hat{n} ds$$

$$M_{12}^{e(^h_e)}(l,k) = \sqrt{Z_e^{(1)}} \left\langle \vec{e}_l^{1e},\ \vec{\Psi}_k^{2(^h_e)} \right\rangle\Big|_{S1} = \sqrt{Z_e^{(1)}} \iint_{S1} \vec{e}_l^{1e} \times \vec{\Psi}_k^{2(^h_e)} \cdot \hat{n} ds$$

$$M_{13}^{(^{hh}_{ee})}(l,k) = \sqrt{Z_{(^h_e)}^{(1)}} \left\langle \vec{e}_l^{1(^h_e)},\ \vec{\Psi}_k^{3(^h_e)} \right\rangle\Big|_{S1} = \sqrt{Z_{(^h_e)}^{(1)}} \iint_{S1} \vec{e}_l^{1(^h_e)} \times \vec{\Psi}_k^{3(^h_e)} \cdot \hat{n} ds$$

$$M_{21}^{h(_e^h)}(l,k) = \sqrt{Z_h^{(2)}} \left\langle \vec{e}_l^{2h}, \vec{\Psi}_k^{1(_e^h)} \right\rangle \Big|_{S2}$$
$$= \sqrt{Z_h^{(2)}} \iint_{S2} \vec{e}_l^{2h} \times \vec{\Psi}_k^{1(_e^h)} \cdot \hat{n} ds$$
$$M_{21}^{e(_e^h)}(l,k) = \sqrt{Z_e^{(2)}} \left\langle \vec{e}_l^{2e}, \vec{\Psi}_k^{1(_e^h)} \right\rangle \Big|_{S2}$$
$$= \sqrt{Z_e^{(2)}} \iint_{S2} \vec{e}_l^{2e} \times \vec{\Psi}_k^{1(_e^h)} \cdot \hat{n} ds$$
$$M_{22}^{h(_e^h)}(l,k) = \sqrt{Z_h^{(2)}} \left\langle \vec{e}_l^{2h}, \vec{\Psi}_k^{2(_e^h)} \right\rangle \Big|_{S2}$$
$$= \sqrt{Z_h^{(2)}} \iint_{S2} \vec{e}_l^{2h} \times \vec{\Psi}_k^{2(_e^h)} \cdot \hat{n} ds$$
$$M_{22}^{e(_e^h)}(l,k) = \sqrt{Z_e^{(2)}} \left\langle \vec{e}_l^{2e}, \vec{\Psi}_k^{2(_e^h)} \right\rangle \Big|_{S2}$$
$$= \sqrt{Z_e^{(2)}} \iint_{S2} \vec{e}_l^{2e} \times \vec{\Psi}_k^{2(_e^h)} \cdot \hat{n} ds$$
$$M_{23}^{h(_e^h)}(l,k) = \sqrt{Z_h^{(2)}} \left\langle \vec{e}_l^{2h}, \vec{\Psi}_k^{3(_e^h)} \right\rangle \Big|_{S2}$$
$$= \sqrt{Z_h^{(2)}} \iint_{S2} \vec{e}_l^{2h} \times \vec{\Psi}_k^{3(_e^h)} \cdot \hat{n} ds$$
$$M_{23}^{e(_e^h)}(l,k) = \sqrt{Z_e^{(2)}} \left\langle \vec{e}_l^{2e}, \vec{\Psi}_k^{3(_e^h)} \right\rangle \Big|_{S2}$$
$$= \sqrt{Z_e^{(2)}} \iint_{S2} \vec{e}_l^{2e} \times \vec{\Psi}_k^{3(_e^h)} \cdot \hat{n} ds$$
$$M_{31}^{(_{ee}^{hh})}(l,k) = -\sqrt{Z_{(_e^h)}^{(1)}} \left\langle \vec{e}_l^{1(_e^h)}, \vec{\Psi}_k^{1(_e^h)} \right\rangle \Big|_{S3}$$
$$= -\sqrt{Z_{(_e^h)}^{(1)}} \iint_{S3} \vec{e}_l^{1(_e^h)} \times \vec{\Psi}_k^{1(_e^h)} \cdot \hat{n} ds$$
$$M_{32}^{h(_e^h)}(l,k) = -\sqrt{Z_h^{(1)}} \left\langle \vec{e}_l^{1h}, \vec{\Psi}_k^{2(_e^h)} \right\rangle \Big|_{S3}$$
$$= -\sqrt{Z_h^{(1)}} \iint_{S3} \vec{e}_l^{1h} \times \vec{\Psi}_k^{2(_e^h)} \cdot \hat{n} ds$$
$$M_{32}^{e(_e^h)}(l,k) = -\sqrt{Z_e^{(1)}} \left\langle \vec{e}_l^{1e}, \vec{\Psi}_k^{2(_e^h)} \right\rangle \Big|_{S3}$$
$$= -\sqrt{Z_e^{(1)}} \iint_{S3} \vec{e}_l^{1e} \times \vec{\Psi}_k^{2(_e^h)} \cdot \hat{n} ds$$
$$M_{33}^{(_{ee}^{hh})}(l,k) = -\sqrt{Z_{(_e^h)}^{(1)}} \left\langle \vec{e}_l^{1(_e^h)}, \vec{\Psi}_k^{3(_e^h)} \right\rangle \Big|_{S3}$$
$$= -\sqrt{Z_{(_e^h)}^{(1)}} \iint_{S3} \vec{e}_l^{1(_e^h)} \times \vec{\Psi}_k^{3(_e^h)} \cdot \hat{n} ds.$$

REFERENCES

[1] C. Kudsia, R. Cameron, and W.-C. Tang, "Innovations in microwave filters and multiplexing networks for communications satellite systems," *IEEE Trans. Microwave Theory Tech.*, vol. 40, pp. 1133–1149, June 1992.

[2] R. H. MacPhie and K.-L. Wu, "Scattering at the junction of a rectangular waveguide and a large circular waveguide," *IEEE Trans. Microwave Theory Tech.*, vol. 43, pp. 2041–2045, Sept. 1995.

[3] N. Yoneda, M. Miyasaki, T. Nishino, and H. Asao, "Analysis of circular-to-rectangular waveguide T-junction using mode-matching technique," *Electron. Commun. Japan*, pt. 2, vol. 80, no. 7, pp. 37–45, 1997.

[4] N. Yoneda, M. Miyazaki, and T. Noguchi, "A 90 GHz-band monoblock type waveguide orthomode transducer," in *Proc. IEEE MTT-S Int. Microwave Symp. Dig.*, 1999, pp. 1781–1784.

[5] P. Krauss and F. Arndt, "Rigorous mode-matching method for the modal analysis of the T-junction circular to sidecoupled rectangular waveguide," in *Proc. IEEE MTT-S Int. Microwave Symp. Dig.*, 1995, pp. 1355–1358.

[6] G. G. Gentili and A. Melloni, "Analysis of the X-junction between two rectangular waveguides and a circular waveguide," *IEEE Microwave Guided Wave Lett.*, vol. 7, pp. 245–247, Aug. 1997.

[7] R. H. MacPhie and K.-L. Wu, "A full-wave modal analysis of arbitrarily shaped waveguide discontinuities using the finite plane-wave series expansion," *IEEE Trans. Microwave Theory Tech.*, vol. 47, pp. 232–237, Feb. 1999.

[8] K.-L. Wu, "An optimal circular-waveguide dual mode filter without tuning screws," *IEEE Trans. Microwave Theory Tech.*, vol. 47, pp. 271–276, Mar. 1999.

[9] E. Kuhn, "A mode-matching method for solving field problems in waveguide and resonator circuits," *Arch. Elektr. Ubertragung*, vol. 27, pp. 511–518, 1973.

Ke-Li Wu (M'90–SM'96) received the B.S and M.Eng degrees from Nanjing University of Science and Technology, Nanjing, China, in 1982 and 1985, respectively, and the Ph.D. degree from Laval University, Quebec, QC, Canada, in 1989.

From 1989 to 1993, he was a Research Engineer and a Research Group Manager with the Communications Research Laboratory, McMaster University. In March 1993, he joined the Corporate Research and Development Division, COM DEV International, Cambridge, ON, Canada, where he had been a Principle Member of Technical Staff in charge of developing advanced electromagnetic design software for various microwave subsystems for communication satellite and wireless communications. Since October 1999, he has been with the Department of Electronic Engineering, The Chinese University of Hong Kong, Shatin, Hong Kong, where he is an Associate Professor. He is also an Adjunct Associate Professor with McMaster University, Hamilton, ON, Canada. He has authored or co-authored numerous publications in the areas of electromagnetic modeling and microwave and antenna engineering. He holds one Canadian patent and one U.S. patent. He contributed to *Finite Element and Finite Difference Methods in Electromagnetics Scattering* (Amsterdam, The Netherlands: Elsevier, 1990) and *Computational Electromagnetics* (Amsterdam, The Netherlands: Elsevier, 1991). His current research interests include all aspects of numerical methods in electromagnetics, various passive microwave circuits, integrated antenna arrays and low-temperature co-fired ceramic (LTCC) multichip modules (MCMs) for wireless communications.

Dr. Wu was the recipient of the 1992 URSI Young Scientist Award. He was also the recipient of the 1993 Industry Feedback Award presented by the Telecommunication Research Institute of Ontario and the 1998 COM DEV Achievement Award.

Ming Yu (S'90–M'93) received the Ph.D. degree in electrical engineering from the University of Victoria, Victoria, BC, Canada, in 1993.

In 1993, he joined COM DEV, Cambridge, ON, Canada, as a Member of Technical Staff. Since then, he has been involved in the design of passive microwave hardware from 500 MHz to 60 GHz, insuring compliance with specifications, cost, and schedules. He was also a Principal Developer of a variety of COM DEV proprietary software for microwave filters and multiplexers. His varied experience also includes being the Manager of Filter/Multiplexer Technology (Space Group) and Manager of Test Engineering and Staff Scientist of Corporate Research and Development. He is currently a Director of Research and Development Programs of the Corporate Research and Development Department, where he oversees the development of RF microelectromechanical system (MEMS) technology, computer-aided tuning and electromagnetic modeling of microwave filters/multiplexers for wireless applications. He has authored or co–authored over 15 publications. He has three patents pending.

Dr. Ming was the recipient of the 1995 COM DEV Achievement Award for the development of a computer-aided tuning (CAT) technique for microwave filters and multiplexers.

Apu Sivadas received the Electrical Engineering degree from the Regional Engineering College, Calicut, India, in 1991, and the Masters and Ph.D. degrees from the Indian Institute of Technology, Kanpur, India, in 1992 and 1997 respectively, all in electrical engineering. His doctoral dissertation concerned modeling and measurements of slotted waveguide array antennas.

He was with Phase Devices Ltd., Dunstable, U.K., where he was involved with comb-line filters for six months. In December 1997, he joined COM DEV Space, Cambridge, ON, Canada, where he was involved with the Multiplexer Product Division and the Corporate Research and Development Department. While with COM DEV, he has also been involved with various filter and multiplexer structures and has contributed significantly to several of the computer-aided design suites for multiplexer and filter design. He has had extensive design experience on circular waveguide dual-mode filters, comblines, and septum and iris filters, in addition to filter network synthesis. Since June 2000, he has been with the GENNUM Corporation, Burlington, ON, Canada, where he is currently a High-Speed Integrated Circuit (IC) Design Engineer involved with data communication products. His current interests include bipolar/CMOS high-speed IC design, IC package characterization, and analog signal processing.